NIST

United States Department of Commerce
Technology Administration
National Institute of Standards and Technology

NISTIR 3990

GRADIOMETER ANTENNAS FOR TUNNEL DETECTION

David A. Hill

GRADIOMETER ANTENNAS FOR TUNNEL DETECTION

David A. Hill

Electromagnetic Fields Division
Electronics and Electrical Engineering Laboratory
National Institute of Standards and Technology
Boulder, Colorado 80303

June 1992

CONTENTS

GRADIOMETER ANTENNAS FOR TUNNEL DETECTION

David A. Hill

Electromagnetic Fields Division
National Institute of Standards and Technology
Boulder, CO 80303

The use of gradiometer antennas for detection of long conductors and detection of empty tunnels is analyzed. For reception in vertical boreholes, the gradiometer consists of two vertical electric or magnetic dipoles with a vertical separation. Both sum and difference responses are useful, but the difference response has the potential advantage of suppressing the primary field and making the scattered field easier to detect. The difference response is most effective in suppressing the primary field for a parallel scan where the transmitting antenna and receiving gradiometer are always at the same height. Gradiometers are most advantageous at low frequencies where the scattered field is small compared to the primary field.

Key words: cylindrical tunnel; electric dipole; electric field; gradiometer; grounded conductor; insulated conductor; magnetic dipole; magnetic field; plane wave.

1. INTRODUCTION

A common problem in electromagnetic detection of tunnels or other subsurface objects is that the scattered field is small compared to the primary field and is therefore difficult to detect. This problem occurs for detection of both empty tunnels and tunnels containing conductors. Several methods have been used to attempt to suppress the primary field: (1) the use of a large separation between transmitting and receiving antennas in the detection of long conductors at low frequencies [1,2], (2) the use of a receiving antenna that is polarized orthogonally to the primary field [3,4], and (3) the use of a gradiometer receiving antenna [5].

This report will consider only the gradiometer method. Stolarczyk [5] has performed low frequency measurements with a gradiometer antenna, and the suppression of the primary field was encouraging. In this report, the theoretical basis of the gradiometer method will be studied. Section 2 covers the application of the method to tunnels containing long conductors,

1

and Section 3 covers the application of the method to empty (air-filled) tunnels.

2. MAGNETIC DIPOLE EXCITATION OF LONG CONDUCTORS

2.1 Formulation

The geometry for excitation of a long conductor by a vertical magnetic dipole is shown in figure 1. An infinitely long conductor of outer radius b is centered on the z axis. A transmitting vertical (y-directed) magnetic dipole of magnetic moment IA is located at (x_d, y_d, z_d). A gradiometer receiving antenna is centered at (x, y, z) and will be described mathematically in eqs (6) and (7). The earth has permittivity ϵ, conductivity σ, and free-space magnetic permeability μ_0. We assume that the magnetic dipole source and the conductor are located at a sufficient depth that the air-earth interface can be neglected.

A vertical magnetic dipole antenna is well suited to detection of horizontal conductors in tunnels because it radiates a horizontal electric field which will excite axial currents in horizontal conductors. A practical vertical magnetic dipole that will fit in boreholes has been constructed using a solenoidal winding on a ferrite core [5]. The gradiometer receiving antenna can be constructed using a pair of such antennas.

The electric and magnetic fields can be derived in terms of a y-directed magnetic Hertz vector, and the derivation is given in [1]. For a vertical magnetic gradiometer receiving antenna, only the vertical magnetic field H_y is required. It can be written as the sum of the primary field H_y^d due to the dipole and the secondary field H_y^c due to the conductor:

$$H_y = H_y^d + H_y^c. \tag{1}$$

2

The primary field is given by [1]

$$H_y^d = \frac{IA\,e^{-jkr_d}}{4\pi r_d} \{k^2[1 - \frac{(y-y_d)^2}{r_d^2}] + \frac{jkr_d + 1}{r_d^2}[\frac{3(y-y_d)^2}{r_d^2} - 1]\},\tag{2}$$

where $k = \omega[\mu_0(\epsilon - j\sigma/\omega)]^{1/2}$ and $r_d = [(x-x_d)^2 + (y-y_d)^2 + (z-z_d)^2]^{1/2}$.

The time dependence is $\exp(j\omega t)$. In general all terms in eq (2) need to be retained.

The secondary magnetic field due to the conductor is [1]

$$H_y^c = \frac{x}{2\pi\rho} \int_{-\infty}^{\infty} \hat{I}(\lambda)\,vK_1(v\rho)\,e^{-j\lambda z}\,d\lambda,\tag{3}$$

where $\rho = (x^2 + y^2)^{1/2}$, $v = (\lambda^2 - k^2)^{1/2}$, and K_1 is the first-order modified Bessel function of the second kind [6]. $\hat{I}(\lambda)$ is the spatial transform of the conductor current and is given by [1]

$$\hat{I}(\lambda) = \frac{IA}{2\pi}[\frac{x_d k^2 K_1(v\rho_{d0})}{\rho_{d0}vD(\lambda)}],\tag{4}$$

where $\rho_{d0} = (x_d^2 + y_d^2)^{1/2}$, $D(\lambda) = K_0(vb) + \frac{2\pi(\sigma+j\omega\epsilon)}{v^2} Z_s(\lambda)$, and $Z_s(\lambda)$ is the axial impedance (series impedance per unit length) of the conductor.

A good model for a conductor in a tunnel is shown in figure 2. It consists of a metal cylinder of radius a surrounded by an insulating region of outer radius b. The metal has conductivity σ_m and magnetic permeability μ_m, and the insulation has permittivity ϵ_i and free-space permeability μ_0. The axial impedance of this model is [1]

$$Z_s(\lambda) = Z_m + \frac{\lambda^2 - k_i^2}{2\pi j \omega \epsilon_i} \ell n(b/a),$$ (5)

where $Z_m = \dfrac{1}{2\pi a} \left(\dfrac{j\omega\mu_m}{\sigma_m}\right)^{1/2} \dfrac{I_0(jk_m a)}{I_1(jk_m a)}$,

$$jk_m = (j\omega\mu_m\sigma_m)^{1/2}, \quad k_i = \omega(\mu_0\epsilon_i)^{1/2},$$

and I_0 and I_1 are modified Bessel functions of the first kind [6]. If we set $b = a$, then $Z_s(\lambda) = Z_m$, and we have a grounded metal conductor (such as a rail in a tunnel). If we set ϵ_i equal to the free-space permittivity ϵ_0, then we can model a conductor (such as a power line) suspended in an air-filled tunnel at a distance $b - a$ from the tunnel wall.

When magnetic field reception is with a pair of magnetic dipole antennas as in figure 1, two outputs (sum and difference) are possible, and Stolarczyk [5] has recorded both as a function of height y. The sum output is proportional to the sum $H_{y\Sigma}$ of the vertical magnetic field at the two dipole heights:

$$H_{y\Sigma}(y) = H_y(y + s/2) + H_y(y - s/2).$$ (6)

In eq (6), we show only the y dependence because both terms are a function of the same x and z coordinates. In a vertical borehole scan, only the y coordinate is varied while x and z are held constant. In a similar manner, the difference output is proportional the difference $H_{y\Delta}$ of the vertical magnetic field at the two dipole heights:

$$H_{y\Delta}(y) = H_y(y + s/2) - H_y(y - s/2).$$ (7)

If s is small, then $H_{y\Delta}$ is given approximately by

4

$$H_{y\Delta}(y) \approx s \; \hat{y} \cdot \nabla H(y), \tag{8}$$

where $\hat{y}$ is a unit vector. Thus $H_{y\Delta}$ is proportional to the y component of the gradient of the magnetic field when s is small, and the pair of magnetic dipoles in the difference mode is called a gradiometer. Under the same condition, $H_{y\Sigma}$ is given approximately by twice the value of $H_y(y)$:

$$H_{y\Sigma}(y) \approx 2 \; H_y(y). \tag{9}$$

For the cases discussed in the following sections, s is not necessarily small, and eqs (6) and (7) are used to generate the numerical results.

2.2 Parallel Scan

In a parallel scan, the source dipole and receiving gradiometer are moved vertically together, and the heights are equal $(y = y_d)$. The advantage of this geometry is that the primary field is cancelled in the difference mode of the gradiometer, and $H_{y\Delta}$ reduces to

$$H_{y\Delta}(y) = [H_y^c(y + s/2) - H_y^c(y - s/2)]\big|_{y_d=y}. \tag{10}$$

Thus the gradiometer in the difference mode responds only to the field scattered by the conductor. In the sum mode, the primary field components add to produce the following result for $H_{y\Sigma}$:

$$H_{y\Sigma}(y) = [2 \; H_y^d(y + s/2) + H_y^c(y + s/2) + H_y^c(y - s/2)]\big|_{y_d=y}. \tag{11}$$

If the primary dipole field H_y^d dominates the secondary conductor field H_y^c, then $H_{y\Sigma}$ is nearly independent of y.

A computer program was written to evaluate $H_{y\Sigma}$ and $H_{y\Delta}$ from eqs (1)-(5), (10), and (11). The λ integration in (3) was evaluated by FFT. In all of the numerical results, we use the following values for the source, conductor, and earth parameters: $IA = 1$ A·m^2, $z_d = 0$, $a = 0.5$ cm, $\sigma_m = 5.7 \times 10^7$ S/m, $\mu_m/\mu_0 = 1$, $\epsilon_i/\epsilon_0 = 1$, $\epsilon/\epsilon_0 = 10$, and $\sigma = 5 \times 10^{-3}$ S/m.

In figures 3 and 4, the magnitudes of $H_{y\Sigma}$ and $H_{y\Delta}$ are shown as a function of y for a conductor midway between the two boreholes ($x = -x_d = 15$ m and $z = 0$). The insulation radius b is set equal to a to model a grounded conductor. In figure 3, the gradiometer separation parameter s is varied from 2 to 20 m. The sum response is only weakly dependent on s, but the difference response has a higher peak value for larger values of s. However, further calculations for values of s larger than 20 m showed a decline in peak value. A perfect null is obtained at $y = 0$, and this null should be easier to detect than the small dip in the sum response. In figure 4, the responses are shown for various frequencies. A frequency of 1 MHz is too high because of increased attenuation in the rock, and a frequency of 10 kHz is too low because of reduced scattering from the conductor. A frequency on the order of 100 kHz is probably optimum for the typical distances involved (30 m borehole separation).

In figure 5, the 30 m borehole separation is maintained, but the conductor passes closer to the source and receiver ($x = -x_0 = 9$ m and $z = 24$ m). The scattered field is larger, and even the sum response shows a significant dip at $y = 0$. In figure 6, both the source and receiver are located on the same side of the conductor ($x_d = -40$ m, $x = -10$ m, and $z = 0$). Here the scattered field is weaker, particularly at 1 MHz, because of the increased attenuation between the source and the conductor.

In figure 7, the effect of the insulation radius b is shown. The scattered field is weaker for larger values of b because the current induced on the conductor [1] is smaller than for the grounded case ($b = a$) shown in figure 3. However the difference response still has its characteristic null at $y = 0$.

Another quantity of interest is the phase of either $H_{y\Sigma}$ or $H_{y\Delta}$ [5]. Figure 8 shows phase results for the same parameters as in figure 3. The phase of $H_{y\Sigma}$ is nearly constant versus y, but the phase of $H_{y\Delta}$ has a 180° jump at y = 0, the location of the null. This rapid phase shift is another possible indicator of the conductor location.

2.3 Diagonal Scan

In a diagonal scan, the source dipole is held fixed, and the receiving gradiometer is moved vertically in a borehole. In a full tomography scan [7,8], this procedure would be repeated for a full range of source heights. In a diagonal scan, the primary field is not completely nulled out, and the general expressions, eqs (6) and (7), are used to calculate $H_{y\Sigma}$ and $H_{y\Delta}$.

In figure 9, magnitude results for a diagonal scan (y_d = 30 m) are shown. Because the dominant primary field is not nulled out, the conductor response does not show up clearly in either $H_{y\Sigma}$ or $H_{y\Delta}$. A weak, displaced null does appear in $H_{y\Delta}$ for the case where the conductor is located closer to the receiving gradiometer (x = 5 m). The phase for this same case is shown in figure 10, and the rapid 180° jump that appeared in figure 8 is reduced and shifted.

For an insulated conductor where the induced current does not attenuate rapidly [1], the total field is dominated by the scattered field for large z. Here the gradiometer can still produce a good null as shown in figure 11 because the primary field is strongly reduced by attenuation in the rock. The null is deeper at z = 200 m than at 100 m. The conductor can also be detected by the maximum in $H_{y\Sigma}$, but the null in $H_{y\Delta}$ is sharper.

3. PLANE WAVE EXCITATION OF EMPTY CIRCULAR TUNNELS

3.1 Formulation

In this section, we consider a circular tunnel model as shown in figure 12. The tunnel of radius a (not to be confused with conductor radius a of section 2) is air filled with permittivity ϵ_0 and permeability μ_0. As in the previous section, the surrounding rock has permittivity ϵ, conductivity σ, and permeability μ_0.

For detection of air-filled tunnels, both polarizations are of interest. For simplicity we consider a plane-wave source rather than a vertical magnetic or electric dipole. The incident plane wave is propagating in the x direction and has either E_z or H_z polarization:

$$E_z^i = E_0 \exp(-jkx) \text{ or } H_z^i = H_0 \exp(-jkx). \tag{12}$$

The total fields for the two polarizations are the sum of the incident and and scattered fields:

$$E_z = E_z^i + E_z^s \text{ or } H_z = H_z^i + H_z^s. \tag{13}$$

The scattered field for E_z polarization is [9-11]

$$E_z^s = E_0 \sum_{m=0}^{\infty} \epsilon_m (-j)^m a_m H_m^{(2)}(k\rho) \cos(m\phi), \tag{14}$$

$$\text{where } a_m = - \frac{k_0 J_m'(k_0 a) J_m(ka) - k J_m(k_0 a) J_m'(ka)}{k_0 J_m'(k_0 a) H_m^{(2)}(ka) - k J_m(k_0) H_m^{(2)\prime}(ka)},$$

$$\epsilon_m = \begin{cases} 1, & m = 0 \\ 2, & m \neq 0 \end{cases}, \quad k_0 = \omega(\mu_0 \epsilon_0)^{1/2},$$

k is given by eq (2), J_m is the mth-order Bessel Function, and $H_m^{(2)}$ is the mth order Hankel function of the second kind [5]. The scattered field for H_z polarization is

$$H_z^s = H_0 \sum_{m=0}^{\infty} \epsilon_m \, (-j)^m \, b_m \, H_m^{(2)}(k\rho) \, \cos(m\phi), \tag{15}$$

$$\text{where } b_m = - \frac{kJ_m'(k_0 a)J_m(ka) - k_0 J_m(k_0 a)J_m'(ka)}{kJ_m'(k_0 a)H_m^{(2)}(ka) - k_0 J_m(k_0)H_m^{(2)}{}'(ka)}.$$

For reception in boreholes, we are interested in the vertical (y-directed) components of the fields. The y components can be obtained from the z components from Maxwell's curl equations. For E_z polarization, the H_y component is given by

$$H_y = \frac{1}{j\omega\mu_0} \frac{\partial E_z}{\partial x}. \tag{16}$$

For H_z polarization, the E_y component is given by

$$E_y = \frac{-1}{\sigma + j\omega\epsilon} \frac{\partial H_z}{\partial x}. \tag{17}$$

By substituting eqs (12)-(15) into eqs (16) and (17) and carrying out the differentiation, we can obtain explicit expressions for H_y and E_y. Convenient normalizations for numerical results are

$$E_0 = -\eta \text{ and } H_0 = 1/\eta, \tag{18}$$

where $\eta = [\mu_0/(\sigma + j\omega\epsilon)]^{1/2}$.

Then the incident fields are the same for the two polarizations, and H_y and E_y can be written

$$\left.\begin{array}{c} H_y \\ E_y \end{array}\right\} = e^{-jkx} + \left\{\begin{array}{c} H_y^s \\ E_y^s \end{array}\right. , \tag{19}$$

where $\left.\begin{array}{c} H_y^s \\ E_y^s \end{array}\right\} = -\dfrac{1}{jk} \sum_{m=0}^{\infty} \left\{\begin{array}{c} a_m \\ b_m \end{array}\right\} \epsilon_m (-j)^m \left[\dfrac{m \sin\phi}{\rho} H_m^{(2)}(k\rho) \sin(m\rho)\right.$

$$\tag{20}$$

$$\left. + k \cos\phi \, H_m^{(2)\prime}(k\rho) \cos(m\phi)\right].$$

Thus, the only difference between the two polarizations is in the scattering coefficient: a_m is associated with H_y^s and b_m is associated with E_y^s. A computer program was written to handle both polarizations simultaneously. Convergence of the m summation in eq (20) is fairly rapid so long as $|k|a$ is not too large.

3.2 Scattered Field

Before performing a numerical evaluation of the scattered fields, it is useful to examine the low frequency behavior. When $k_0 a$ and $|k|a$ are small, the Bessel functions in a_m and b_m can be replaced by their small argument expansions [6]. For E_z polarization, the leading scattering coefficient is

$$a_0 \approx (j\pi/4)(k^2 - k_0^2)a^2. \tag{21}$$

Then the leading term in H_y^s is

10

$$H_y^s \approx -(\pi/4) \ (k^2 - k_0^2) a^2 \ \cos\phi \ H_0^{(2)'}(k\rho). \tag{22}$$

The $(k^2 - k_0^2) a^2$ dependence in eq (22) indicates that the scattering from an electrically small, empty tunnel is very weak. This is quite different from E_z scattering from an electrically small, highly conducting cylinder where the scattering is strong [12].

For H_z scattering, the leading scattering coefficient is

$$b_1 \approx (j\pi/4) \ (k^2 - k_0^2) a^2, \tag{23}$$

which is equal to a_0 in eq (21). The leading term in E_y^s is

$$E_y^s \approx (j\pi/2) \ (k^2 - k_0^2) a^2 \ [\frac{\sin^2\phi}{k\rho} H_1^{(2)}(k\rho) + \cos^2\phi \ H_1^{(2)'}(k\rho)]. \tag{24}$$

The computer program was found to agree with eqs (22) and (24) for sufficiently low frequencies.

For all of the numerical results for the empty tunnel, we choose the following parameters: $a = 1$ m, $\epsilon/\epsilon_0 = 1$, and $\sigma = 5 \times 10^{-3}$ S/m. In figure 13, we show the magnitudes of the y components of the total fields as a function of y at $x = 5$ m. At 10 MHz, the scattered field is weak, and the total field is nearly constant at the incident field value of $\exp(-jkx)$. At 50 MHz, the circumference of the tunnel is approximately equal to a free-space wavelength, and the scattering is fairly strong. The two dips in the total field (for both polarizations) have been discussed by other authors [9,13] in tunnel detection applications. Further calculations show strong scattering for most frequencies above 50 MHz, but weak scattering for frequencies below about 20 MHz.

Calculations for larger values of x show weaker scattered fields and more nearly constant total fields. This model is not well suited to analyzing the far-field (large x) behavior of the total field because the

plane-wave incident field has no spreading loss while the scattered field has inverse square root distance spreading loss. A better model for examining the far-field behavior would have either a line source or a dipole source. In these cases the incident field and scattered field would have the same spreading loss.

3.3 Gradiometer Response

Since the field scattered from an empty tunnel at low frequencies is weak compared to the primary field, we again examine the possibility of using a gradiometer receiving antenna to suppress the primary field. For E_z polarization, H_y is the vertical field component that can be received most easily in a borehole. The gradiometer antenna for this case has already been described in section 2, and the sum and difference responses are proportional to $H_{y\Sigma}$ and $H_{y\Delta}$ as given in eqs (6) and (7).

For H_z polarization, E_y is the vertical component that can be received. in a vertical borehole. In this case the two receiving antennas shown in figure 12 are vertical electric dipoles. The sum and difference responses are proportional to $E_{y\Sigma}$ and $E_{y\Delta}$ which are given by

$$E_{y\Sigma}(y) = E_y(y + s/2) + E_y(y - s/2) \tag{25}$$

and
$$E_{y\Delta}(y) = E_y(y + s/2) - E_y(y - s/2). \tag{26}$$

In figures 14 and 15, we show the gradiometer responses at 10 MHz for s = 2 m and 5 m. In both cases the sum response shows little variation with y, but the difference response shows the characteristic null at y = 0. The peak values are greater for s = 5 m. Also, the H_z polarization (vertical E_y) produces a stronger scattered field and difference response. This is consistent with scattered field calculations by others.

Figure 16 shows gradiometer responses at 50 MHz. Here the scattered field is strong enough that both the sum and difference responses show

12

enough y variation to indicate the tunnel height. For such cases with strong scattering, it is not clear whether the gradiometer provides a significant advantage over a single dipole antenna.

Figure 17 shows gradiometer responses for the case where the receiving antennas are located on the lit side of the tunnel (x = -5 m) rather than on the shadow side. Here the scattered field is reduced, the difference response is reduced, and the sum response shows almost no y variation.

4. CONCLUSIONS

The results presented in sections 2 and 3 indicate that a gradiometer receiving antenna is useful in suppressing the primary field and allowing the field scattered by an empty tunnel or a conductor in a tunnel to be observed in the absence of the primary field. The typical gradiometer response has a null at the height of the tunnel due to symmetry and symmetrical peaks above and below. These features occur most prominently with a parallel scan, rather than with a diagonal scan where the primary field is not completely nulled out.

The best frequencies for detection of long conductors are in the vicinity of 100 kHz, and this is unchanged from earlier results with single dipole receivers [1,2]. The spacing between the two vertical dipole receivers that form the gradiometer is not critical, but too small a spacing reduces the received difference to too low a level. Too large a spacing broadens the distance between the two peaks and degrades the vertical resolution. Spacings on the order of 2 to 10 m yield good results.

For detection of empty tunnels, either vertical or horizontal polarization can be used. Thus the source and gradiometer can use either vertical electric or vertical magnetic dipoles in boreholes. Stronger scattering is obtained for vertical polarization using vertical electric dipoles. Frequencies of 50 MHz or higher yield strong scattering that should be detectable with either a single antenna or a gradiometer. When strong scattering is obtained, it is not as clear whether a gradiometer receiver has a significant advantage over a single dipole receiver. However, there is always some advantage because the sum response is

13

approximately the same as the response of a single dipole and the difference response provides additional information. If lower frequencies on the order of 10 MHz are used, gradiometers are useful in suppressing the primary field and allowing the weak scattered field to be detected. Normally the reason for using lower frequencies is to increase range.

Further study of several issues involving gradiometer antennas would be useful. The idealized theoretical scans for gradiometers show a perfect null with symmetrical peaks above and below, but preliminary measurements [5] do not show such deep nulls. Models with less symmetry, such as noncircular tunnels [14] or tunnels with multiple conductors, could be studied to determine asymmetry effects on gradiometers. Imperfect alignment and spacings of the gradiometer dipoles could degrade the null, and these effects could be studied. We assumed a plane-wave source in the empty tunnel analysis, but a more realistic source (such as a vertical dipole) would be useful in predicting the proper field decay with distance. Earth layering or inhomogenieties could also be studied to obtain an estimate of the effects of geologic noise [15-18] on gradiometer response. The gradiometers studied here utilize the vertical variation of the vertical field component, but other variations and field components could also be useful in improving the ratio of the received scattered field to primary field if other receiving geometries could be employed in boreholes.

5. ACKNOWLEDGMENTS

6. REFERENCES

[1] Hill, D.A. Magnetic dipole excitation of a long conductor in a lossy medium. IEEE Trans. Geosci. Rem. Sens., GE-26: 720-725; 1988.

[2] Hill, D.A. Magnetic dipole excitation of an insulated conductor of finite length. IEEE Trans. Geosci. Rem. Sens., GE-28: 289-294; 1990.

[3] Bollen, R.L. Tunnel detection by low-frequency magnetic-field emissions and the controlled source audio magneto telluric techniques. SRI International: January 1989.

[4] Hill, D.A. Near-field and far-field excitation of a long conductor in a lossy medium. Nat. Inst. Stand. Tech. (U.S.) NISTIR 3954; 1990.

[5] Stolarczyk, L.G. Evaluation of RIM system II instruments, data acquisition methods, and data processing algorithms for detection of shallow and deeply buried tunnels with and without electrical conductors. Stolar Inc.: May 1991.

[6] Abramowitz, M.; Stegun, I.A. Handbook of Mathematical Functions with Formulas, Graphs, and Mathematical Tables. Nat. Bur. Stand. (U.S.) AMS 55; 1964.

[7] Shope, S.; Greenfield, R.J. Electromagnetic cross-hole tomography for tunnel detection. Third Technical Symposium on Tunnel Detection. Golden, CO: January 12-15, 1988.

[8] Frank, M.S.; Balanis; C.A. Electromagnetic tomography in tunnel detection. Third Technical Symposium on Tunnel Detection. Golden, CO: January 12-15, 1988.

[9] Lee, T.K.; Kim, S.Y.; Ra, J.W. Resonant scattering of cw electromagnetic wave by an underground tunnel of circular cross-section. Third Technical Symposium on Tunnel Detection. Golden, CO: January 12-15, 1988.

[10] Jones, D.S. The Theory of Electromagnetism. Oxford: Pergamon Press, 1964.

[11] Van de Hulst, H.C. Light Scattering by Small Particles. New York: Wiley; 1957.

[12] Harrington, R.F. Time-Harmonic Electromagnetic Fields. New York: McGraw-Hill; 1961.

[13] Lee, T.K.; Park, S.O.; Ra, J.W. Near-field diffraction pattern by an underground void of circular cylinder. Microwave Opt. Tech. Let., 2: 179-183; 1989.

[14] Lytle, R.J.; Laine, E.F.; Lager, D.L.; Davis, D.T. Cross-borehole electromagnetic probing to locate high-contrast anomalies. Geophys., 44: 1667-1676; 1979.

[15] Hill, D.A.; Wait, J.R. Theoretical noise and propagation models for through-the-earth communication. National Telecommunications and Information Administration; May 1992.

[16] Eaton, P.A.; Hohmann, G.W. An evaluation of electromagnetic methods in the presence of geologic noise. Geophys., 52: 1106-1126; 1987.

[17] Greenfield, R. Borehole radar clutter. National Radio Science
Meeting: Boulder, CO; January 4-6, 1989.

[18] Hill, D.A. Clutter models for subsurface electromagnetic applications.
Nat. Inst. Stand. Tech. (U.S.) NISTIR 89-3909; 1989.
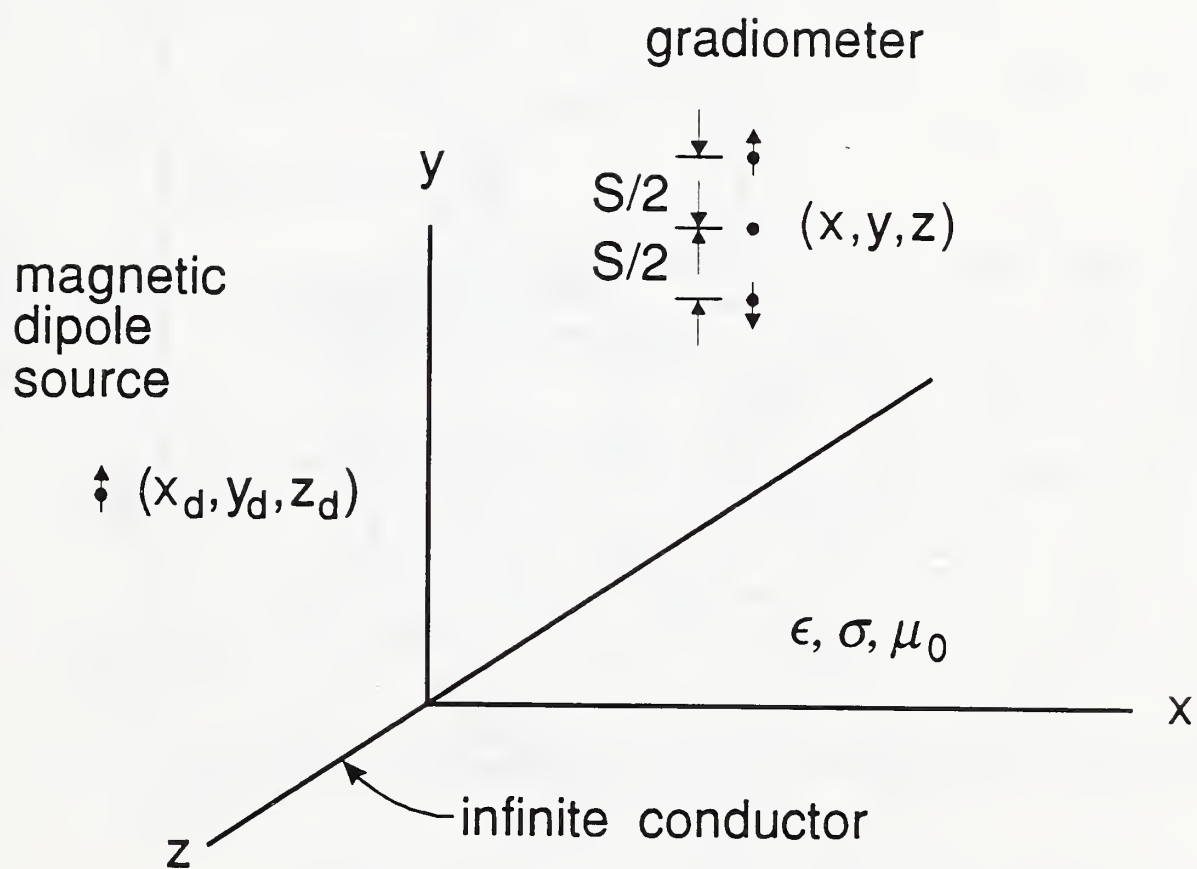
Figure 1.   Geometry   for   an infinitely long conductor excited by a vertical
magnetic   dipole.   The   gradiometer   receiver   consists   of   two
vertical magnetic dipoles separated by a distance s.
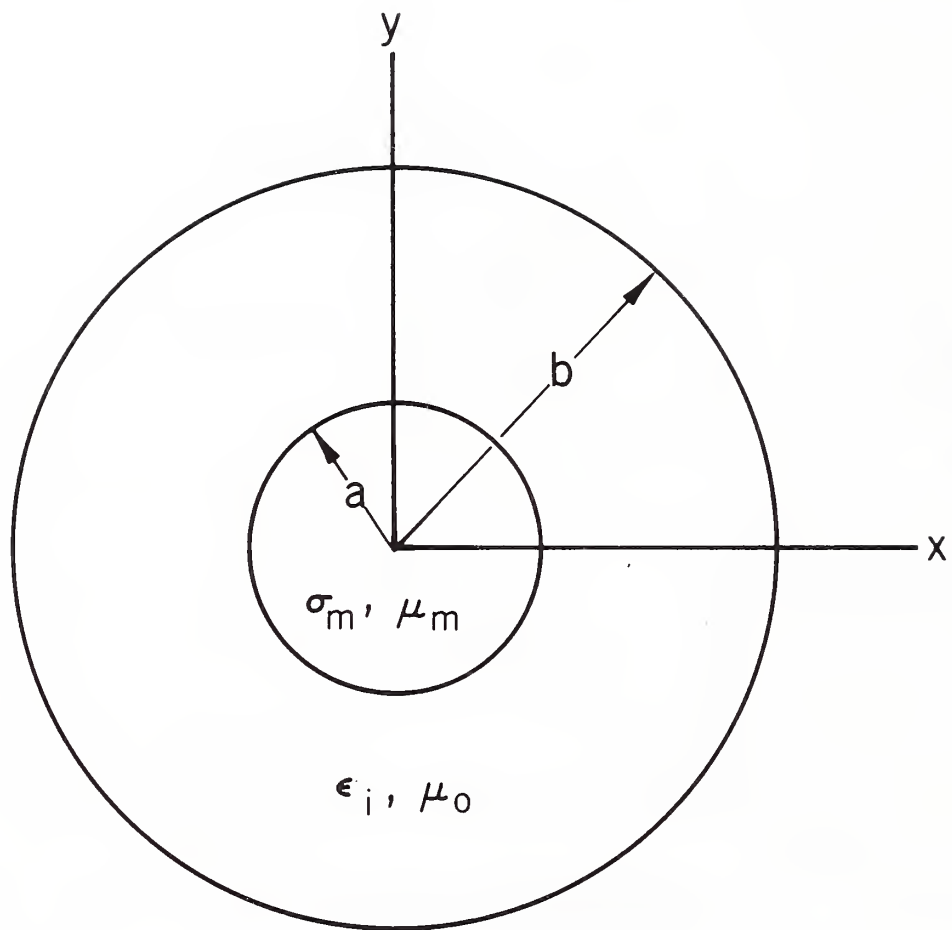
Figure 2. Geometry for an insulated conductor.
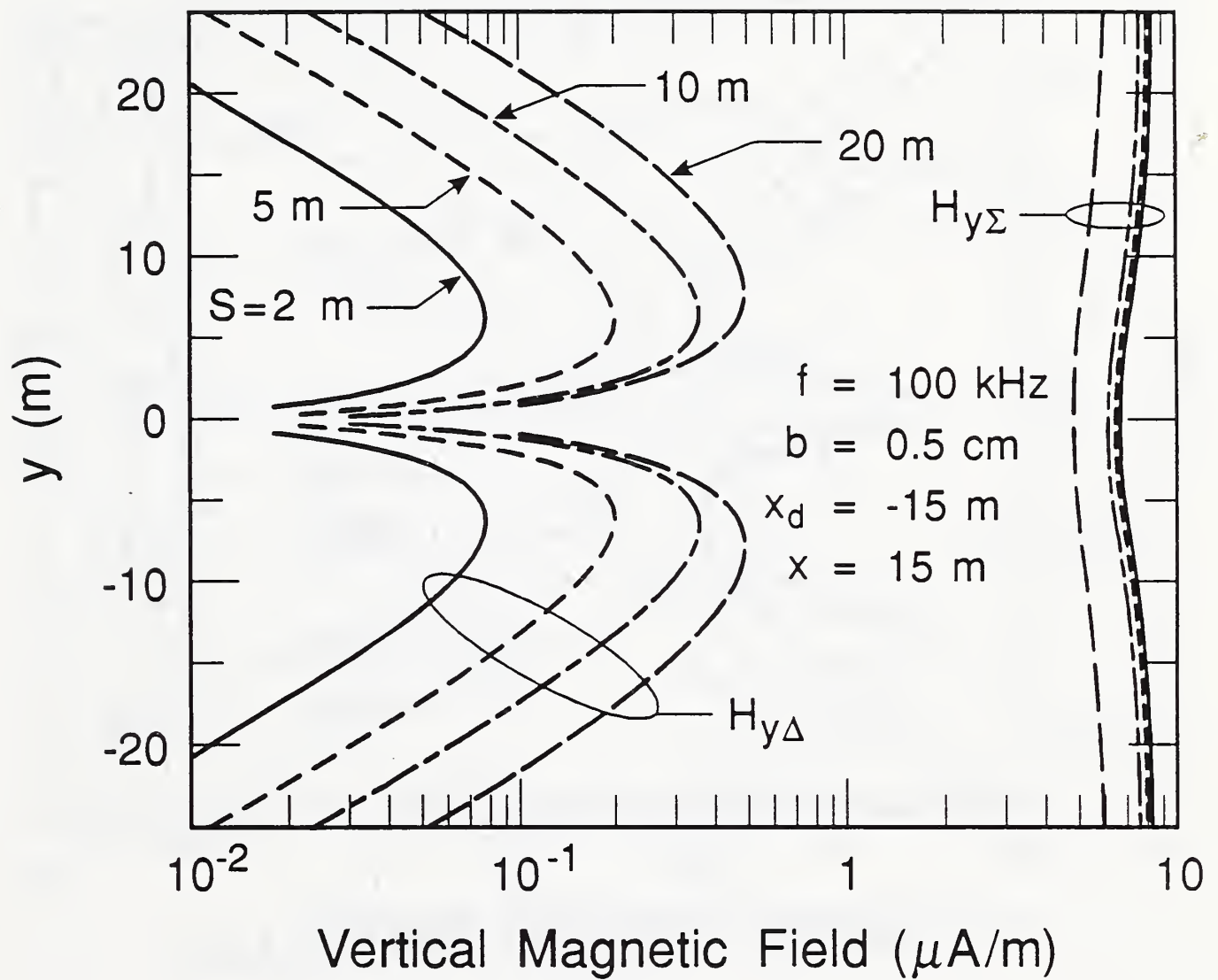
Figure 3. Magnitude of magnetic field gradiometer responses for different values of dipole separation s.
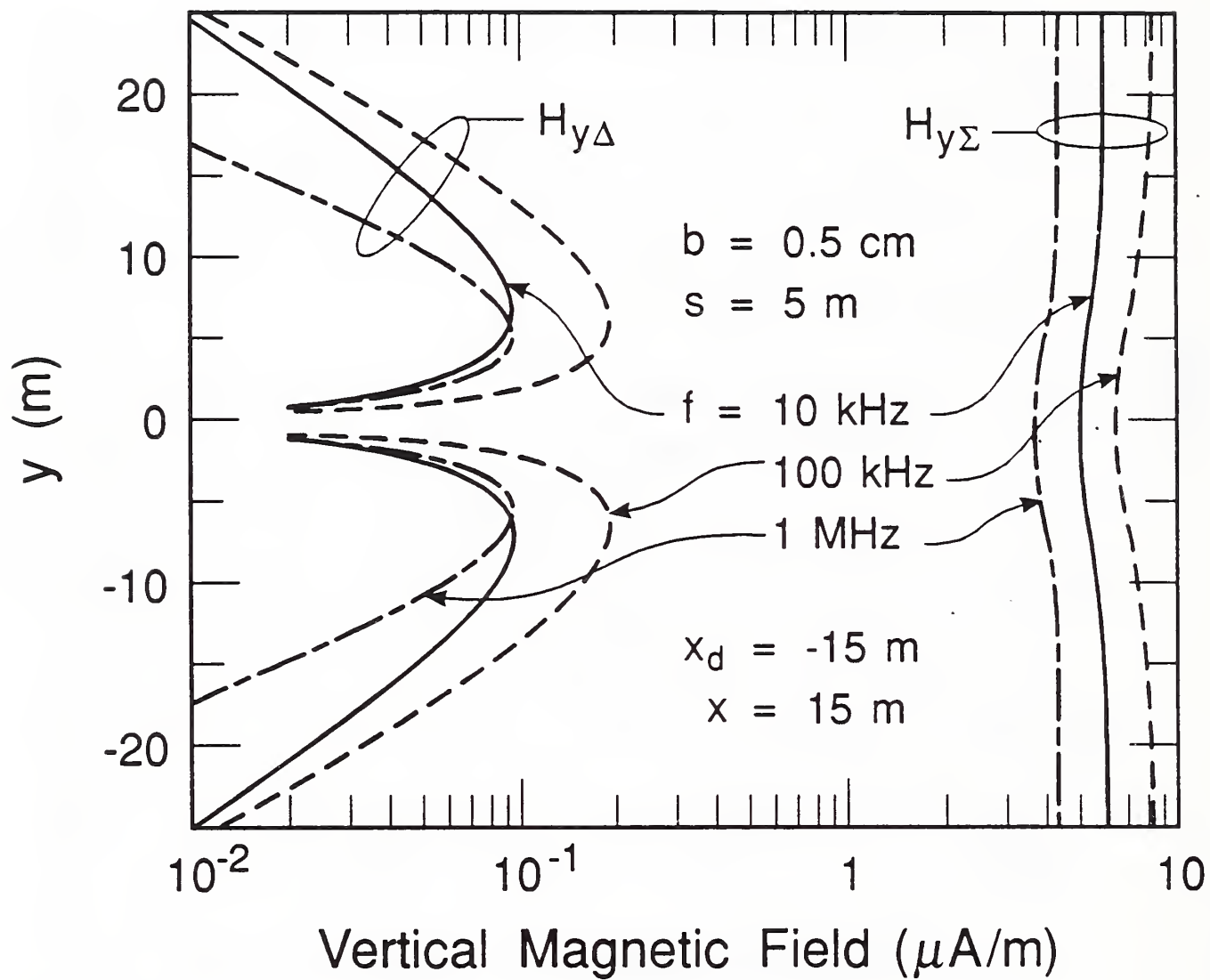
Figure 4. Magnitude of magnetic field gradiometer responses for various frequencies.
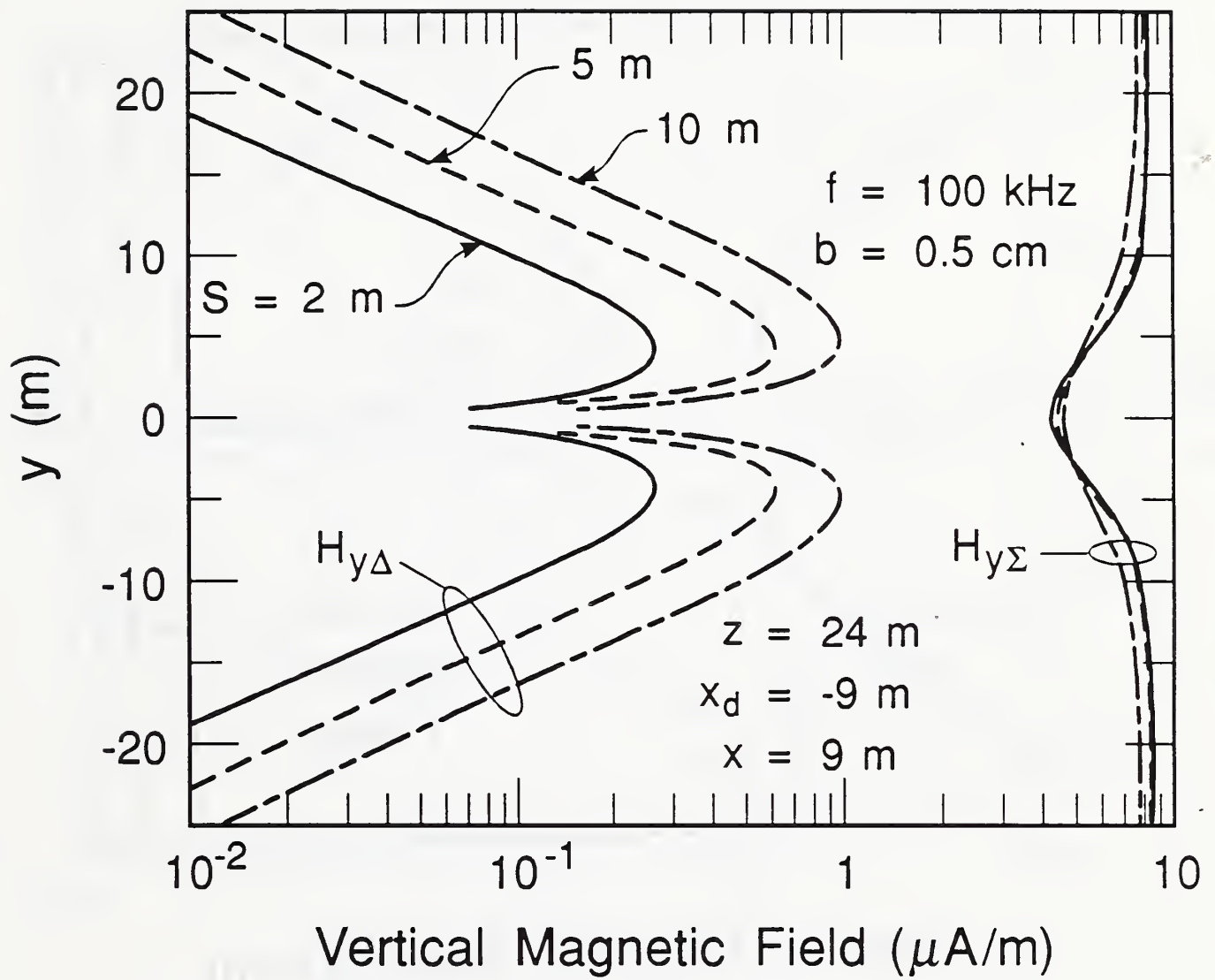
Figure 5. Magnitude of magnetic field gradiometer responses for conductor closer to dipole source and gradiometer.
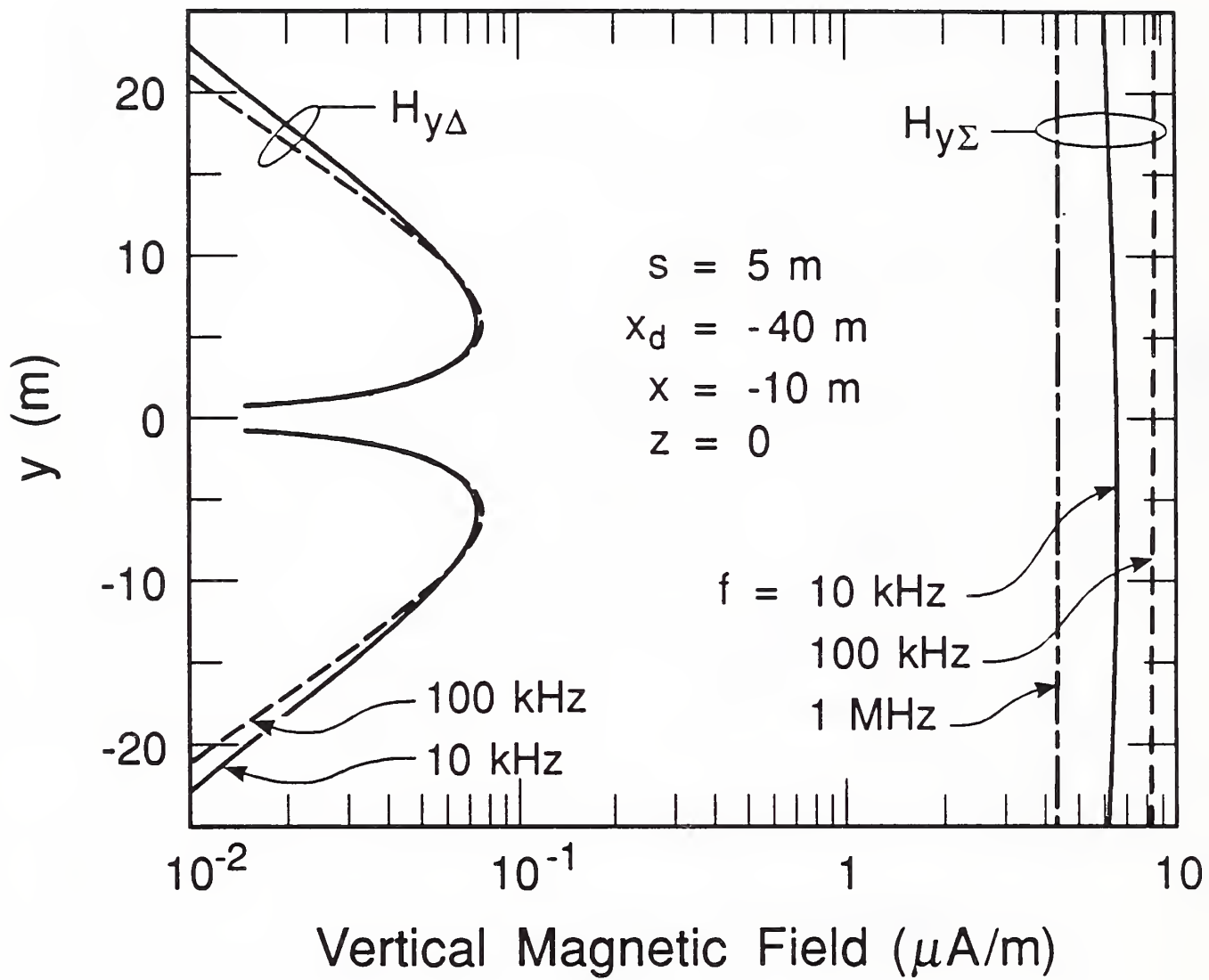
Figure 6. Magnitude of magnetic field gradiometer responses for dipole source and gradiometer on the same side of conductor.
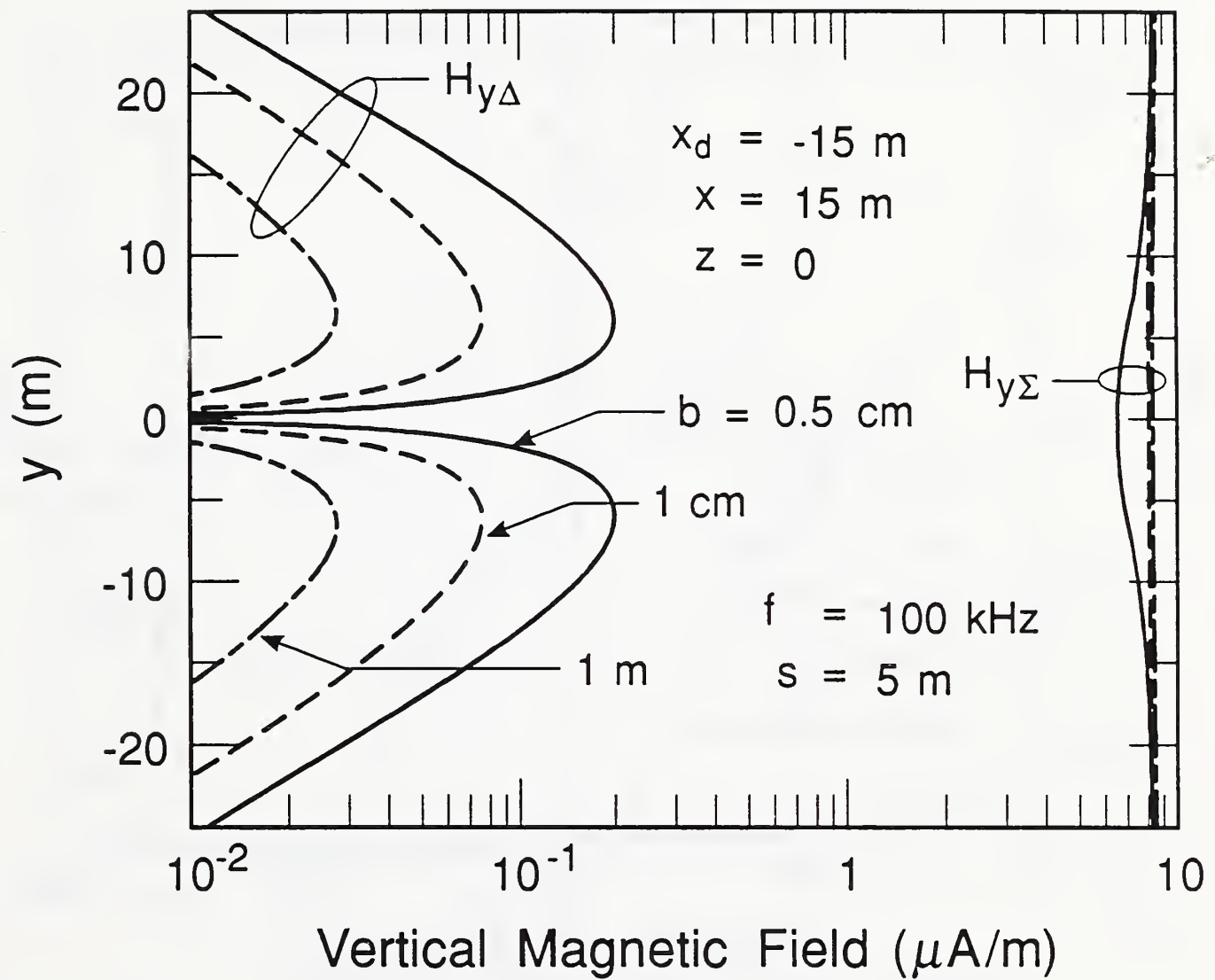
Figure 7. Magnitude of magnetic field gradiometer responses for various values of insulation radius b.
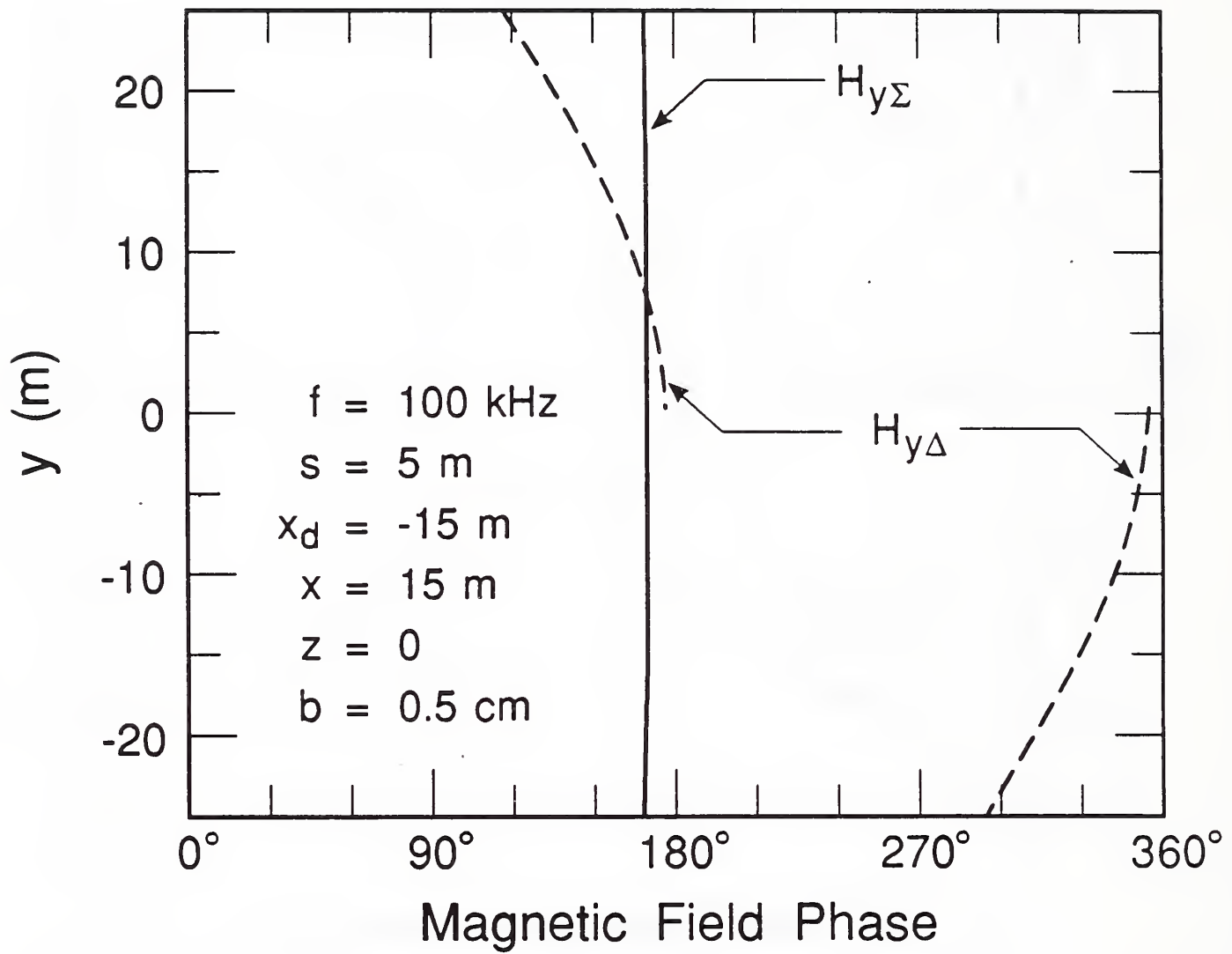
Figure 8. Phase of magnetic field gradiometer responses.
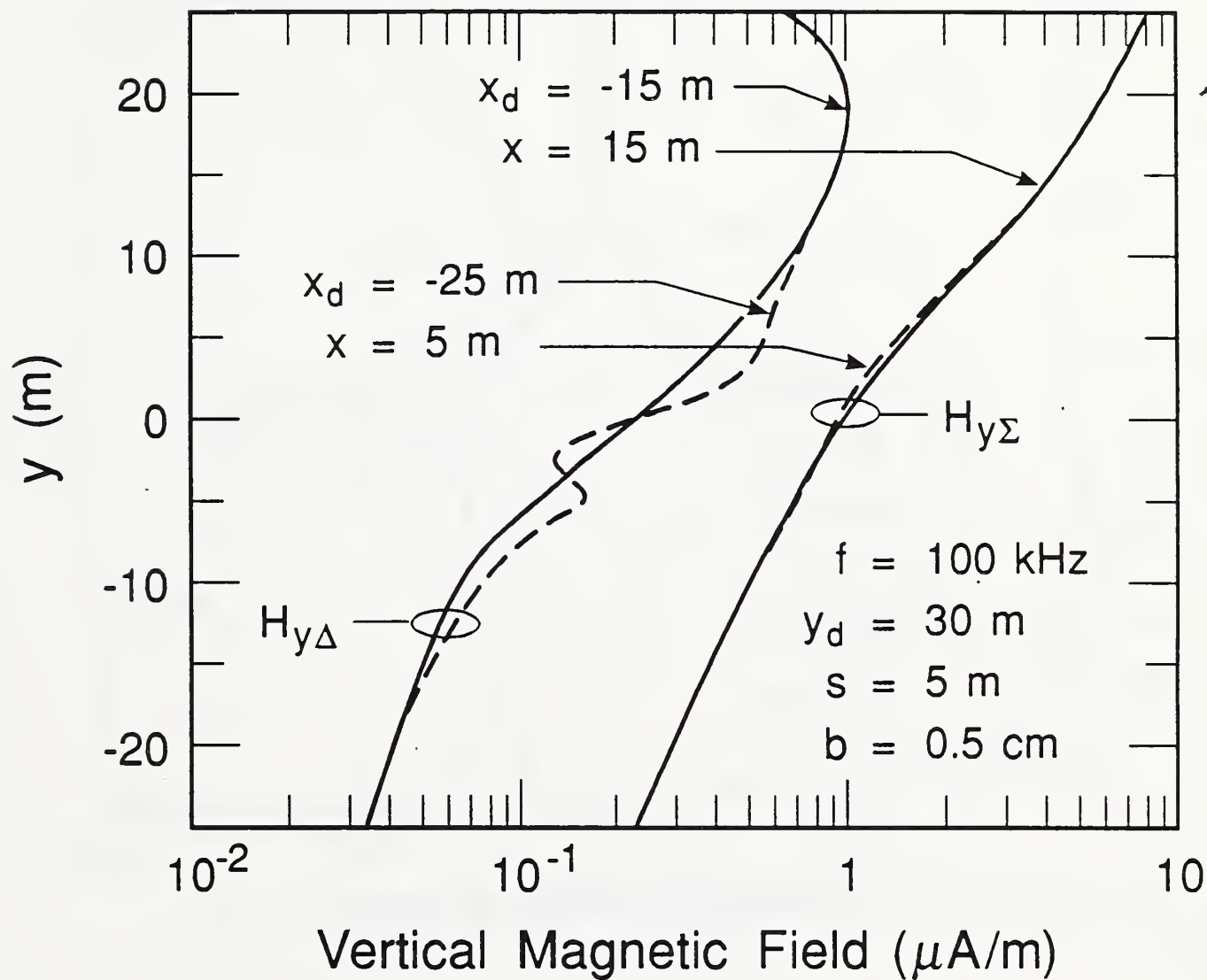
Figure 9. Magnitude of magnetic field gradiometer responses for a diagonal scan.
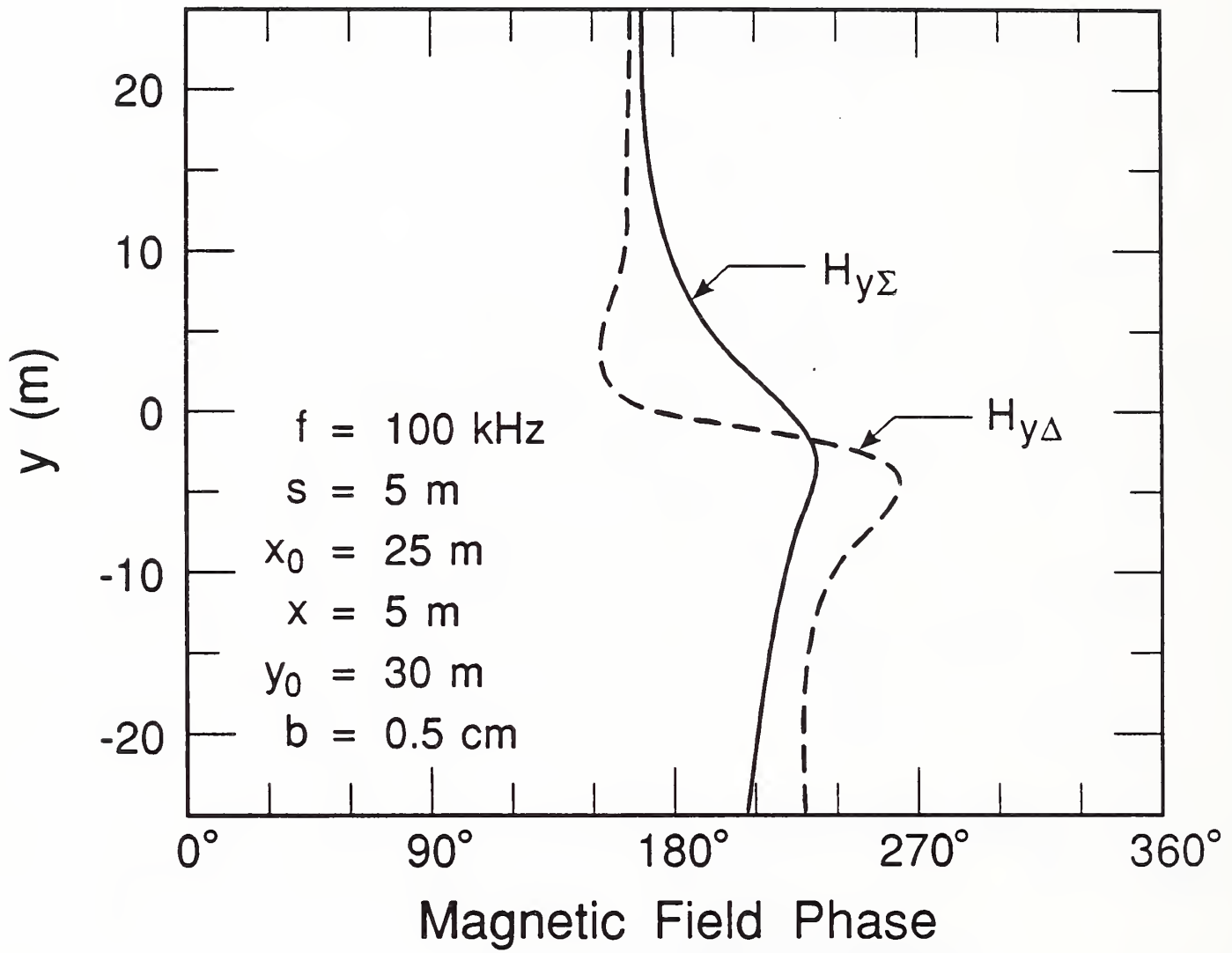
Figure 10. Phase of magnetic field gradiometer responses for a diagonal scan.
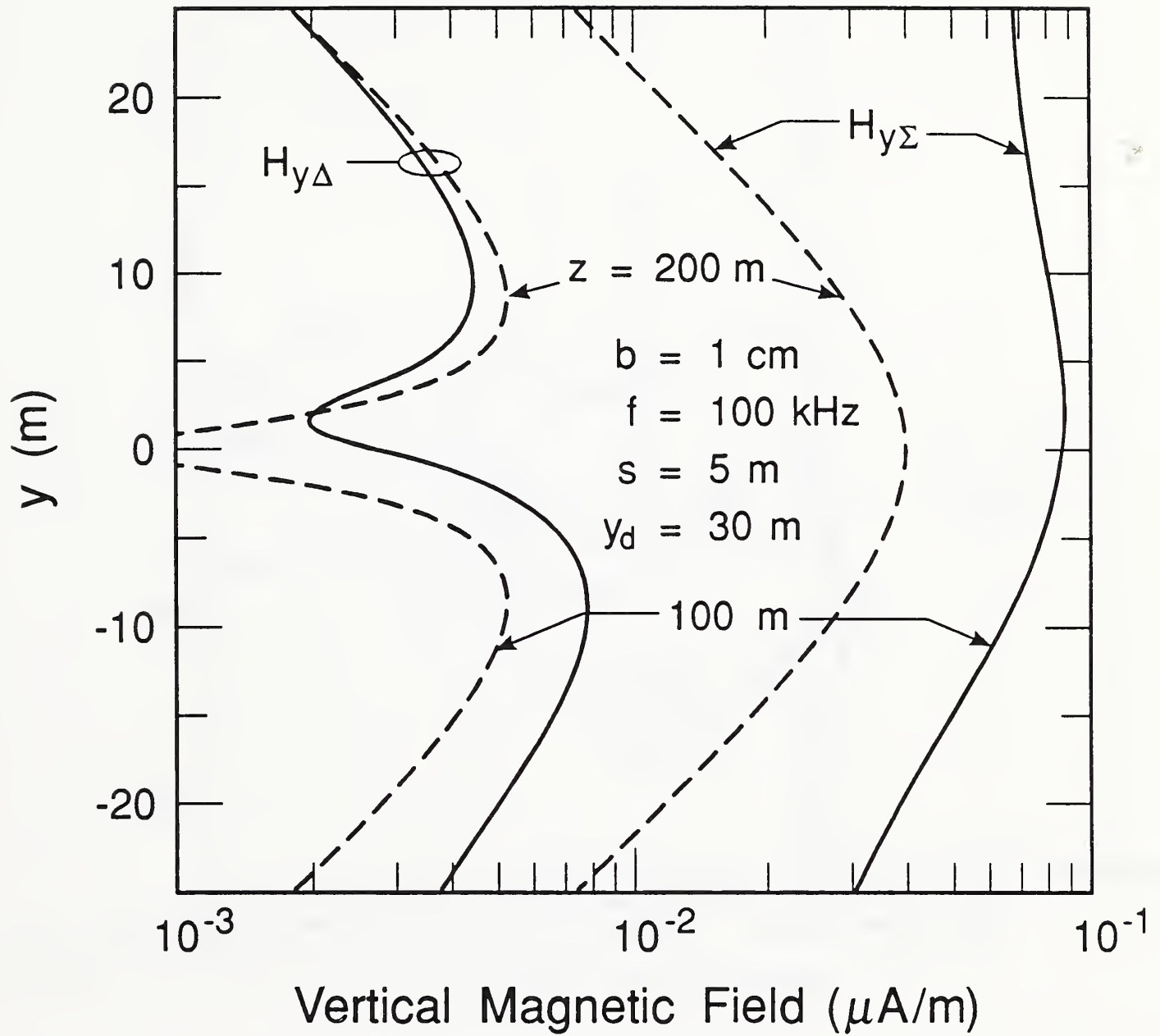
Figure 11. Magnitude of magnetic field gradiometer responses for large z.
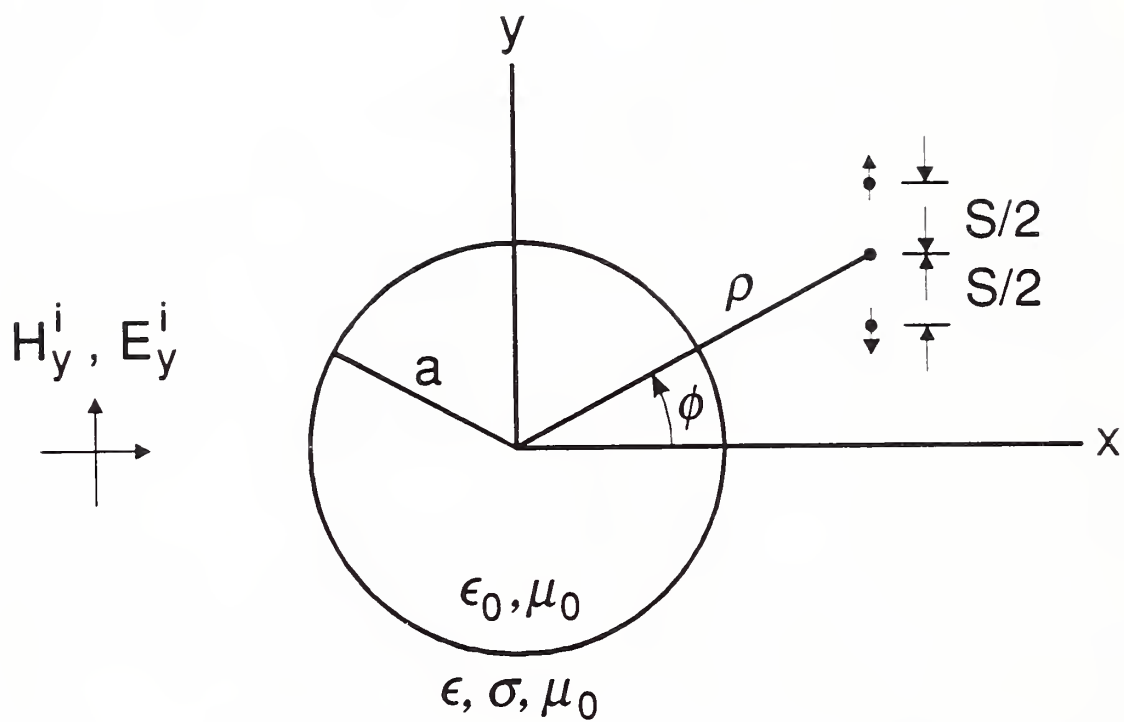
Figure 12. Geometry for a plane wave incident on an empty, circular tunnel. The gradiometer consists of two vertical electric or magnetic dipoles.
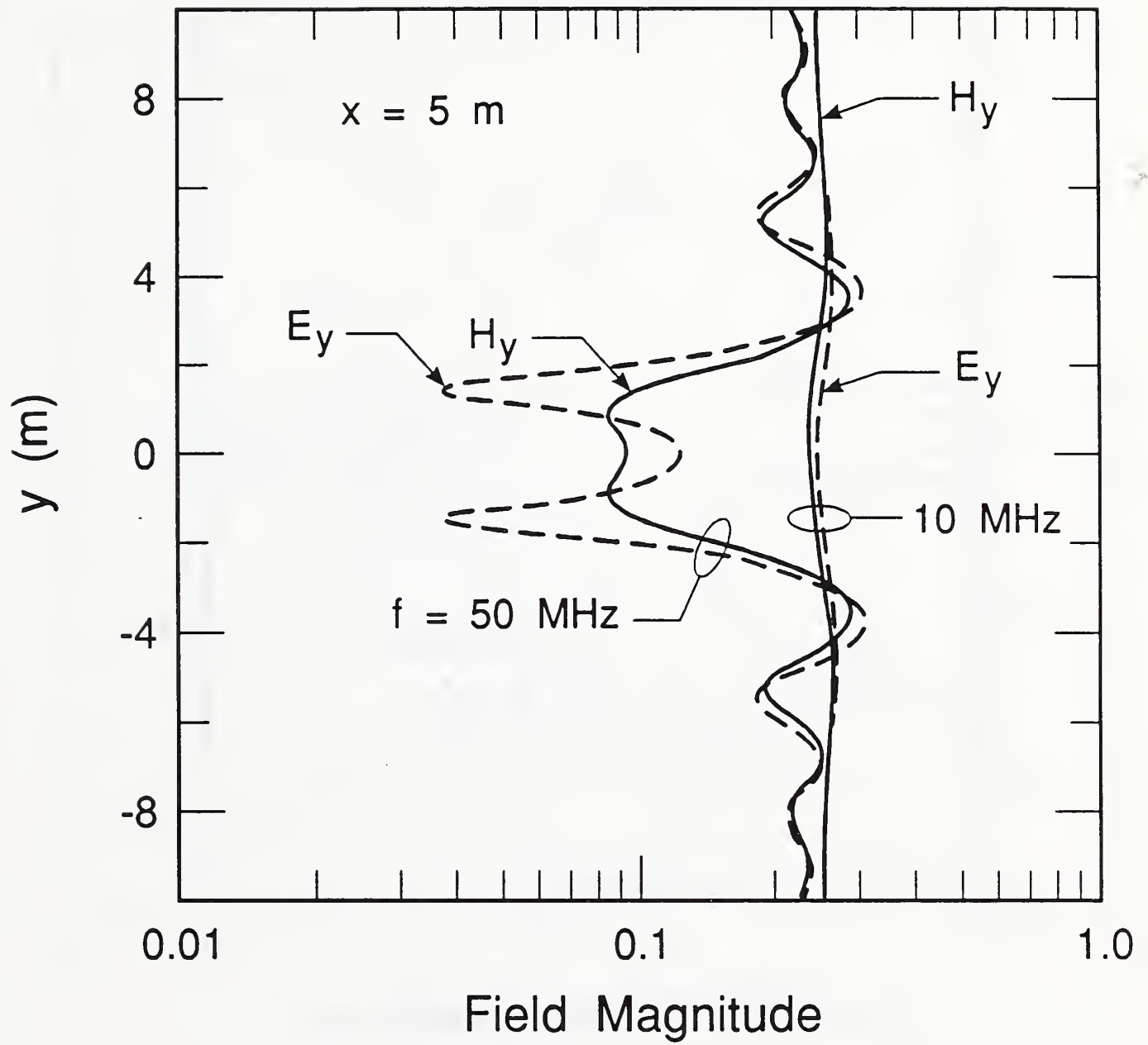
Figure 13. Field magnitudes on the shadow side of an empty tunnel.
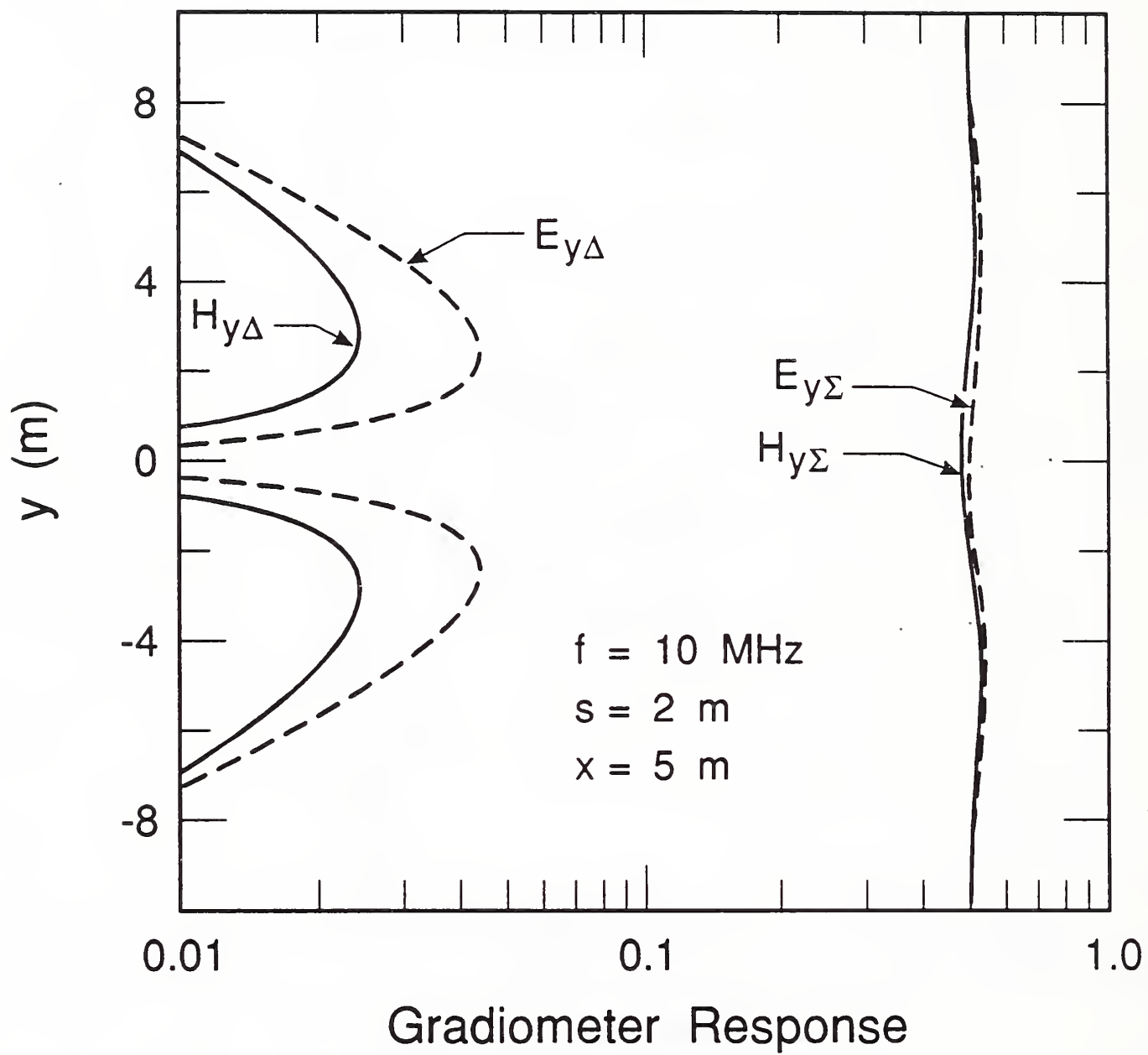
Figure 14. Magnitude of gradiometer responses on the shadow side of an empty tunnel at 10 MHz.
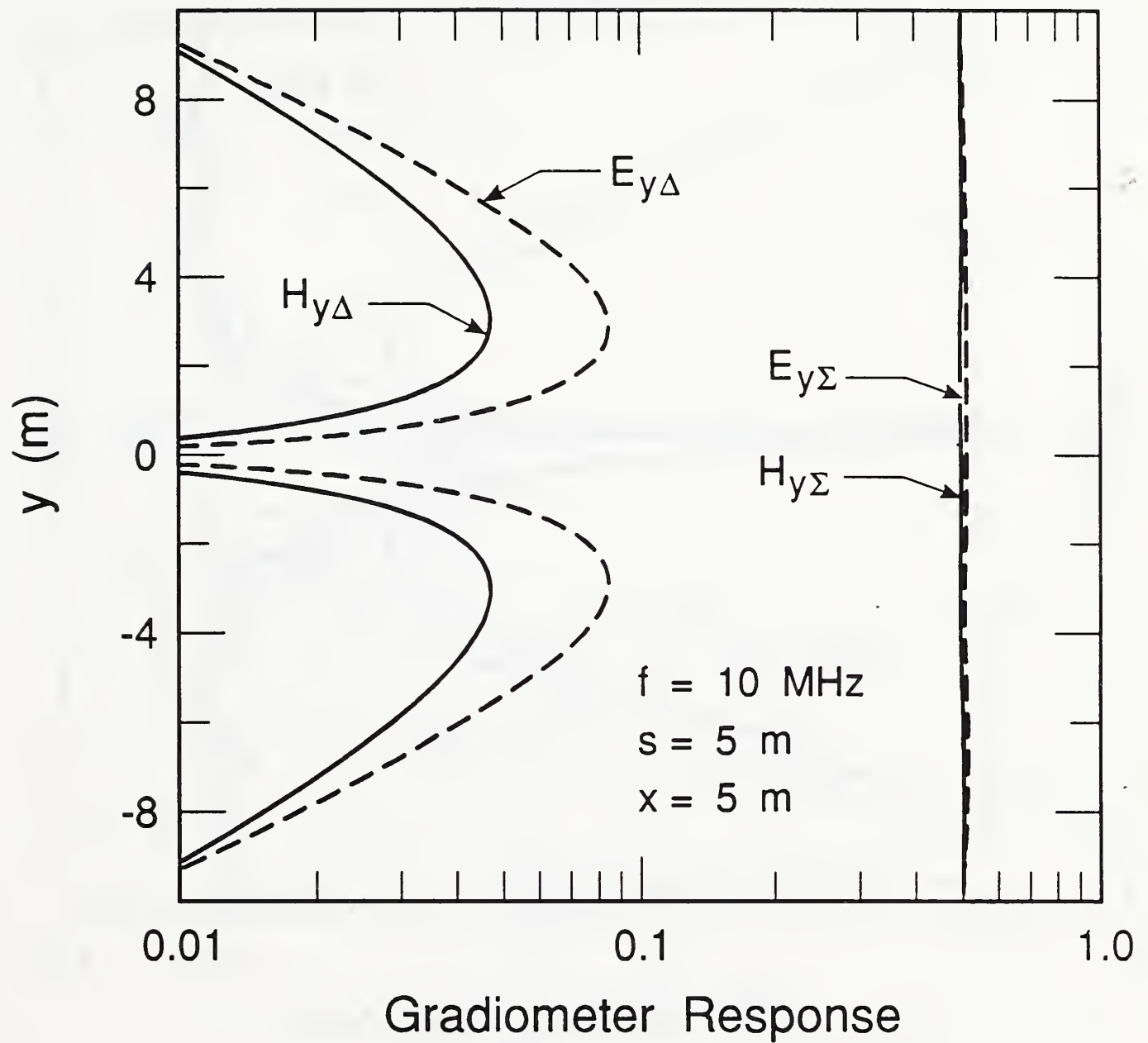
Figure 15. Magnitude of gradiometer responses on the shadow side of an empty tunnel for a larger dipole separation s.
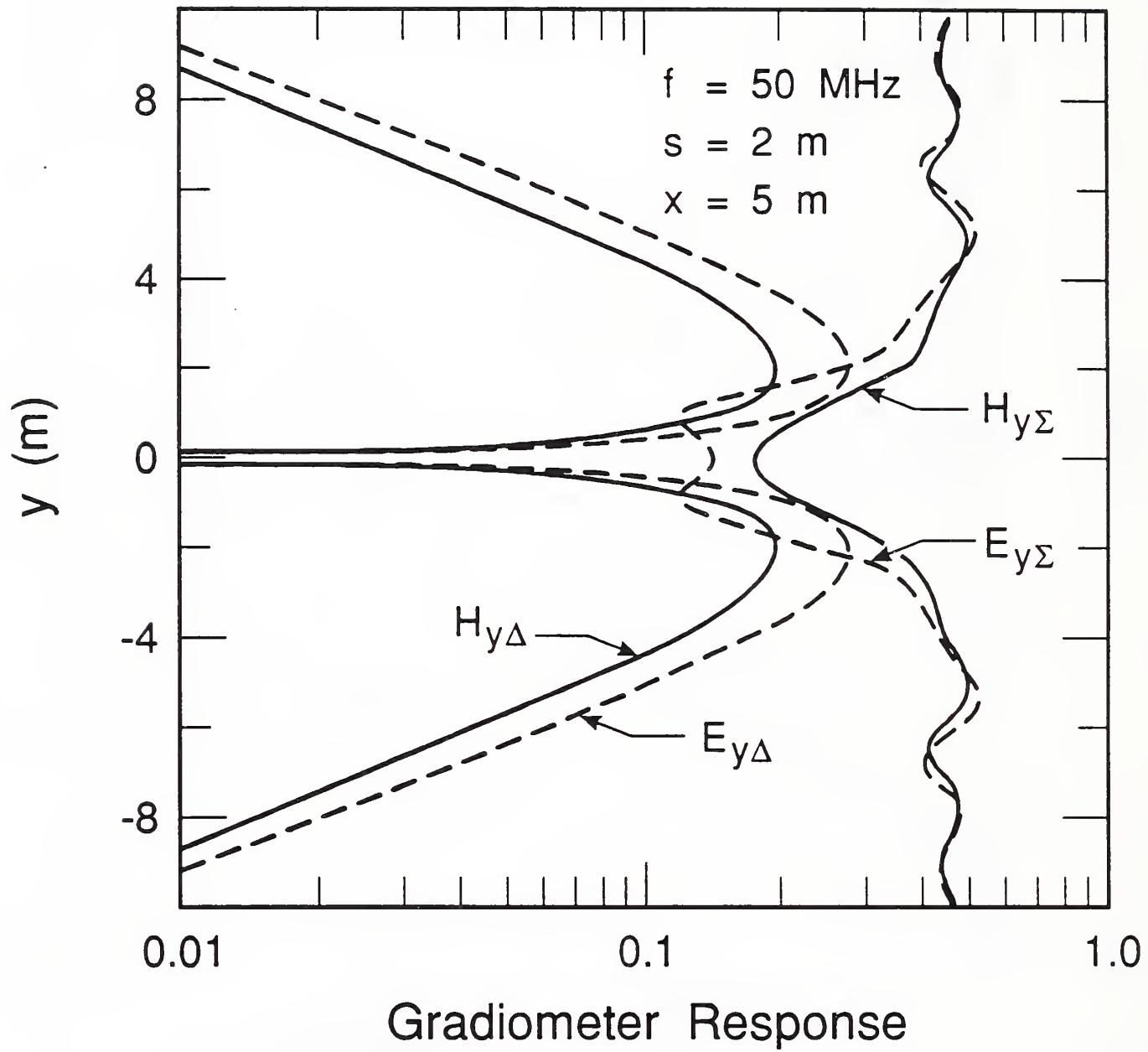
Figure 16. Magnitude of gradiometer responses on the shadow side of an empty tunnel at 50 MHz.
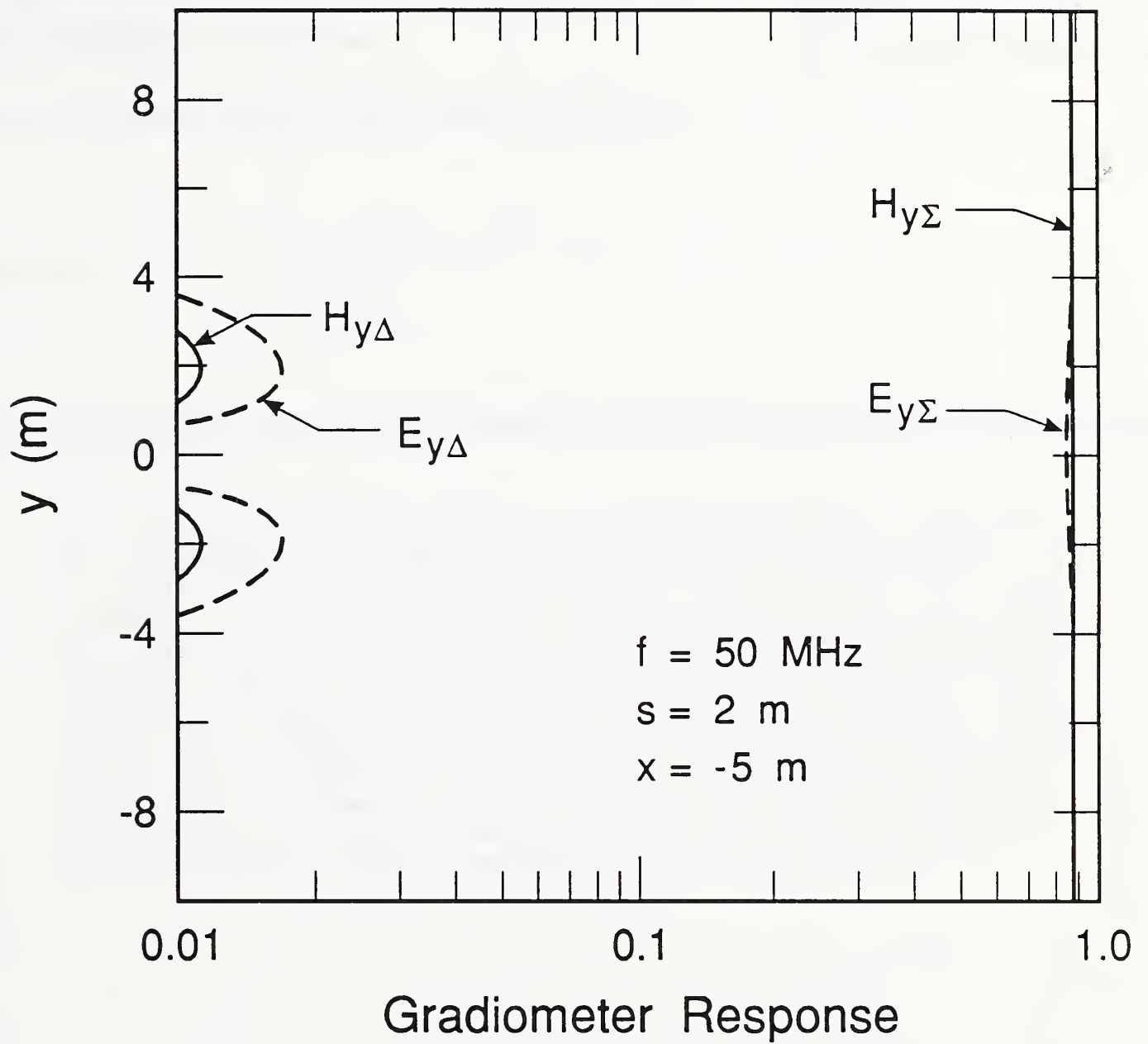
Figure 17. Magnitude of gradiometer responses on the lit side of an empty tunnel at 50 MHz.

4. TITLE AND SUBTITLE

Gradiometer Antennas for Tunnel Detection

5. AUTHOR(S)

David A. Hill

11. ABSTRACT (A 200-WORD OR LESS FACTUAL SUMMARY OF MOST SIGNIFICANT INFORMATION. IF DOCUMENT INCLUDES A SIGNIFICANT BIBLIOGRAPHY OR LITERATURE SURVEY, MENTION IT HERE.)

The use of gradiometer antennas for detection of long conductors and detection of empty tunnels is analyzed. For reception in vertical boreholes, the gradiometer consists of two vertical electric or magnetic dipoles with a vertical separation. Both sum and difference responses are useful, but the difference response has the potential advantage of suppressing the primary field and making the scattered field easier to detect. The difference response is most effective in suppressing the primary field for a parallel scan where the transmitting antenna and receiving gradiometer are always at the same height. Gradiometers are most advantageous at low frequencies where the scattered field is small compared to the primary field.

12. KEY WORDS (6 TO 12 ENTRIES; ALPHABETICAL ORDER; CAPITALIZE ONLY PROPER NAMES; AND SEPARATE KEY WORDS BY SEMICOLONS)

cylindrical tunnel; electric dipole; electric field; gradiometer; grounded conductor; insulated conductor; magnetic dipole; magnetic field; plane wave